Surface engineering of organic nanoparticles for highly improved bioimaging

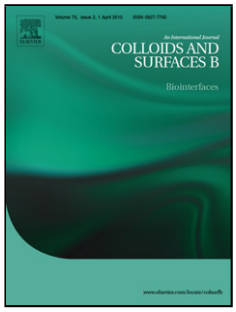

Title: Surface Engineering of Organic Nanoparticles for Highly Improved Bioimaging

Authors: Yanqiu Liu, Xiujuan Zhang, Mengjiao Zhou, Xianfeng Chen, Xiaohong Zhang

PII: S0927-7765(17)30500-3
DOI: http://dx.doi.org/doi:10.1016/j.colsurfb.2017.07.077
Reference: COLSUB 8740

To appear in: *Colloids and Surfaces B: Biointerfaces*

Received date: 13-4-2017
Revised date: 17-7-2017
Accepted date: 27-7-2017

Please cite this article as: Yanqiu Liu, Xiujuan Zhang, Mengjiao Zhou, Xianfeng Chen, Xiaohong Zhang, Surface Engineering of Organic Nanoparticles for Highly Improved Bioimaging, Colloids and Surfaces B: Biointerfaceshttp://dx.doi.org/10.1016/j.colsurfb.2017.07.077

Surface Engineering of Organic Nanoparticles for Highly Improved Bioimaging

Yanqiu Liu,[a] Xiujuan Zhang,[a,*] Mengjiao Zhou,[a] Xianfeng Chen,[b,*] and Xiaohong Zhang[a,*]

[a]Institute of Functional Nano & Soft Materials (FUNSOM) and Jiangsu Key Laboratory for Carbon-Based Functional Materials & Devices, Soochow University, Suzhou Jiangsu, 215123 (P. R. China). E-mail: xjzhang@suda.edu.cn; xiaohong_zhang@suda.edu.cn. Fax: +86-10-65882846. Tel: +86-512-65880955.

[b]Institute for Bioengineering, School of Engineering, University of Edinburgh, Edinburgh EH9 3JL, United Kingdom.

The total number of words in the article is 5464, and the total number of figures is 6.

Graphical abstract:

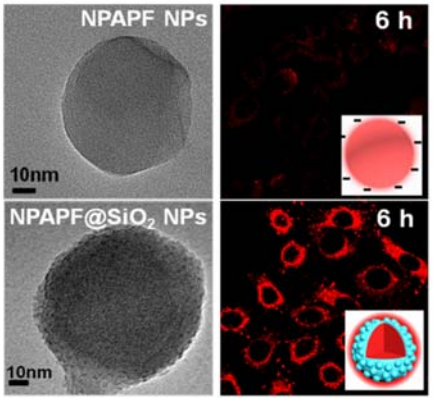

Highlights

- Surface engineering of dye nanoparticles can dramatically induce over ten-fold enhancement in bioimaging brightness.
- Specific non-clathrin- and non-caveolae-mediated pathway is observed.
- Enhanced cellular uptake efficacy and decreased cellular excretion endow dye nanoparticles with superior bioimaging performance.

Abstract

Surface properties of nanoparticles (NPs) have a huge influence on their biological activities. In this work, we report to use mesoporous silica nanoshell surface to regulate the cellular internalization rate and intracellular fate of fluorescent organic NPs for highly improved cellular imaging. We systematically studied the internalization of the NPs into cells, the intracellular transport pathways, the excretion from cells, and very importantly, compared the results with those from various NPs with different surface properties. It was found that the silica nanoshell coating allow the NPs to achieve strikingly improved brightness in imaging (over ten-fold enhancement) and much higher delivery efficiency than other NPs. This was attributed to their unique non-

clathrin- and non-caveolae-mediated pathways which enable them to enter cells very efficiently and quickly in the cellular internalization, as well as their low cellular excretion rate. This highly effective cellular imaging effect caused by silica surface coating is much desirable for applications in sensitive imaging and long-term tracking of cells.

Keywords: fluorescent dye nanoparticles; organic fluorescence probes; mesoporous silica nanoshell; cellular internalization efficiency; cellular imaging

1. Introduction

Fluorescent cellular probes are powerful tools for studying complex biological structures, cellular behaviors and physiological functions. In the past decades, organic dyes are the most widely used fluorescent markers for biological imaging. However, they often suffer from either severe photobleaching at low concentrations or fluorescence quenching at high concentrations [1]. To overcome this issue, recently, pure dye nanoparticles (NPs) with unique characteristic of aggregation induced emission enhancement (AIEE) emerged as a promising new fluorescent probe for bioimaging applications [2]. This material can achieve enhanced fluorescence emission with remarkable photostability and excellent biocompatibility, but the brightness of these NPs still needs to be improved for effective use. The reason is that high sensitivity is usually determined by the brightness of a probe's fluorescence and counted as an essential requirement for optimum imaging and tracking of cells and biological tissues. Clearly, strategies are needed to enhance the brightness of the fluorescent dyes in bioimaging.

Recent observations demonstrate that surface properties of nanocarriers can regulate their dye-loading capacities [3-5] as well as biological activities [6-10]. For example, NPs with positive surface charge are observed to exhibit enhanced cellular internalization comparing to neutral and negatively charged NPs [11]. Silica NPs with surface topography similar to virus are reported to lead to enhanced drug loading capacity of siRNA and cellular uptake efficacy [12]. Nanodiamonds with sharp edges are also found to be able to easily break the endosomal membranes and reside in cytoplasm without being excreted [13]. All these observations indicate that surface properties can exert great influence on cellular internalization rate and the fate of nanomaterials in cells, both of which have significant implications for bioimaging. It is well known that fluorescence NPs with combined features of high cellular internalization and low excretion rate can be enduringly remained within cells [14], and thus the fluorescence intensity can be greatly preserved for sensitive detection.

Motived by these findings, we encapsulated fluorescent organic NPs with a few nanometers thick layer of mesoporous silica. We then systematically studied the internalization of these NPs into cells, the intracellular transport pathways, and the excretion from cells, and very importantly, compare the results with those from various NPs with different surface properties. We expect that this type of organic dye NPs will play an important role in live cell imaging.

2. Experimental

2.1. Materials

N-phenyl-substituted amine, 4-bromophenylacetonitrile, $Pd(OAc)_2$, Cs_2CO_3, P(t-Bu)$_3$, PEI, PSS, TBADN, cethyltrimethylammonium bromide (CTAB), tetramethylorthosilicate (TMOS), and 3-aminopropyltriethoxysilane (APTES) were purchased from J&K Scientific Ltd. Triethylamine, toluene, iodine, diethyl ether, sodium, methanol, chloroform, dichloromethane and petroleum ether were ordered from Sinopharm Chemical Reagent Co Ltd. LysoTracker Green DND-2 were purchased from Invitrogen. Albumin Bovine V (BSA), fetal bovine serum (FBS), Roswell Park Memorial Institute-1640 (RPMI-1640) medium, Dulbecco's Modified Eagle's medium (DMEM) and penicillin-streptomycin solution were purchased from Invitrogen (San Diego, CA). MTT was purchased from Sigma Aldrich (Milwaukee, WI). Distilled water was obtained from a Milli-Q Biocel (Millipore Corporation, Breford, USA) water purification system (18.2 $M\Omega \bullet cm^{-1}$ resistivity). HeLa cells and KB cells were purchased from American Type Culture Collection (ATCC, Manassas, VA, USA). The fluorescence spectra were performed on a FluoroMax 4 (Horiba Jobin Yvon) spectrofluorimeter. SEM images were obtained on a FEI Quanta 200 FEG field emission scanning electron microscope operated at an accelerating voltage of 30 KV. TEM images were taken by FEI Tecnai G2 F20 S-TWIN operated at an accelerating voltage of 200 kV. The NPs' size and surface charge measurements were performed on a Zetasizer Nano ZS (Malvern Instruments, Malvern, U.K.) with a 633 nm He-Ne laser. Cell imaging studies were taken by confocal laser scanning microscopy (CLSM, TCS SP5 II, Leica, Germany).

2.2. Synthesis of NPAPF (TBADN) NPs and NPAPF (TBADN)@SiO_2 NPs

NPAPF was synthesized according to literature [2]. NPAPF and TBADN NPs were individually synthesized by a solvent exchange method. Briefly, NPAPF (TBADN) was dissolved in THF to make a 1×10^{-3} M NPAPF (TBADN) solution. Then 150 μL of solutions were dropped into 5 mL of ultrapure water by microsyringe at room temperature under rapid stirring for 5 min. The resulting NPs dispersion was kept at 4 °C for further use.

NPAPF@SiO_2 NPs and TBADN@SiO_2 NPs were prepared as following. 50 mg of CTAB was added into 30 mL of the above prepared NPAPF (TBADN) NPs solution followed by active stirring of 30 min to make an oil-in-water microemulsion. The suspension was then heated up to 40 °C and kept for 10 min under rapid stirring. A transparent NPAPF (TBADN)/CTAB solution was acquired. Next, 100 μL of 2 M NaOH solution was added into the mixture to make an alkaline environment. Subsequently, 0.1 mL of TMOS and 1 mL of ethylacetate were added into the reaction solution in sequence. After 10 min, 30 μL of APTES was added and the mixture was allowed for reaction for 12 h. To detach CTAB from the NPAPF (TBADN)@SiO_2 NPs, HCl solution was added to control the pH to be ~2.0 and then refluxed for 3 h at 60 °C. The as-synthesized NPAPF (TBADN)@SiO_2 NPs were washed three times with ultrapure water by centrifugation, to remove the unreacted species. Finally, the mixture was under ultrasonic treatment and then stored at 4 °C for further use.

2.3. Surface modification and characterization of NPAPF (TBADN) NPs and NPAPF (TBADN)@SiO_2 NPs

Sizes and surface charges of the NPAPF (TBADN) NPs were measured on Zetasizer Nano ZS with a 633 nm He-Ne laser at room temperature. Both the sizes and surface charges of the NPs were expressed as the average values of three measurements. In order to achieve opposite surface charges for NPAPF NPs and NPAPF@SiO_2 NPs, PEI and PSS were separately added into the as-prepared NPAPF NPs and NPAPF@SiO_2 NPs through electrostatic adsorption. Stewing for 1 h, the unabsorbed PEI and PSS were removed by centrifugation. Finally, four types of particles with different surface structure and charge were prepared and named as NPAPF NPs(-), NPAPF NPs-PEI(+), NPAPF@SiO_2 NPs(+), and NPAPF@SiO_2 NPs-PSS(-).

2.4. Cell culture

HeLa and KB cells were individually cultured in DMEM and RPMI-1640 medium supplemented, containing 10% (v/v) FBS and 1% (v/v) penicillin-streptomycin solution at 37 °C in a humidified atmosphere containing 5% CO_2.

2.5. *In vitro* cytotoxicity

The *in vitro* cytotoxicity was measured using a standard MTT assay. HeLa cells were seeded in 96-well plates (100 μL/well) and incubated for 24 h. Then, 25 μL of sterilized NPAPF NPs(-), NPAPF NPs-PEI(+), NPAPF@SiO_2 NPs(+) and NPAPF@SiO_2 NPs-PSS(-) with different concentrations in DMEM medium were added to each well for incubation (37 °C, 5% CO_2). After 48 h, the cells were then treated with 20 μL of MTT solution (5 mg mL^{-1} in PBS) and incubated for extra 4.5 h. The medium was removed and the cells were lysed by adding 150 μL of DMSO, cell viabilities were then measured by MTT assay.

2.6. Cellular uptake of NPAPF (TBADN) NPs

HeLa or KB cells were dispersed in 24-well plates (1 mL in each well containing 1 × 10^4 cells per well) and cultured for 24 h at 37 °C in the humidified atmosphere with 5% CO_2. Subsequently, HeLa (KB) cells were incubated in NPAPF NPs(-), NPAPF NPs-PEI(+), NPAPF@SiO_2 NPs(+) and NPAPF@SiO_2 NPs-PSS(-) ([NPAPF] = 5 μM) at 37 °C for 2, 4, and 6 h. Cells were then washed with PBS for three times to fully remove nonspecifically absorbed dye and fixed with fresh 4% paraformaldehyde for 5 min at room temperature, and then visualized under CLSM. The emission was collected in the range of 580-680 nm for NPAPF NPs. For TBADN NPs, the excitation was 405 nm and the emission was detected from 420 to 480 nm. All images were captured under the same instrumental setting and analyzed with image analysis software.

To acquire quantitative data, the fluorescence intensities were measured by flow cytometry. HeLa cells were seeded in 6-well plates and incubated for 24 h, and then NPAPF NPs were added and incubated for 2, 4, and 6 h. The cells were washed with PBS and harvested by trypsinization. Subsequently, the cells were centrifuged at 1000 rpm for 3 min and re-suspended in 0.5 mL of DMEM medium for analysis by flow cytometry. NPAPF was detected with an excitation wavelength at 488 nm and an emission wavelength at 650 nm.

2.7. Protein adsorption

To determine protein adsorption, 1 mL of NPAPF NPs(-), NPAPF NPs-PEI(+), NPAPF@SiO_2 NPs(+) and NPAPF@SiO_2 NPs-PSS(-) solution, 3 mL of ultrapure water and 1 mL of 4 mg/mL BSA were added together and stirred vigorously with a

magnetic stirrer for 4 h. The NPAPF particles were centrifuged and the concentration of BSA was determined in the supernatant using UV-visible absorption spectra by determining the absorbance maximum at 280 nm wavelength. A standard curve was prepared using known concentrations of BSA. The protein adsorbed on the different NPAPF NPs was calculated using following equation:

$$\mathbf{q} = (\mathbf{C_i}\text{-}\mathbf{C_f})\mathbf{V}/\mathbf{m}$$

where $\mathbf{C_i}$ and $\mathbf{C_f}$ are the initial BSA concentration and the BSA concentration in the supernatant after adsorption studies, respectively; **V** is the total volume of the solution (5 mL); and **m** is the mass of the NPs added into the solution.

2.8. Mechanism of NPAPF NPs internalization into cells

Effect of energy on the cellular uptake of NPAPF NPs was studied by pre-incubating HeLa cells at 4 °C for 1 h, and then incubated with NPAPF NPs(-), NPAPF NPs-PEI(+), NPAPF@SiO_2 NPs(+) and NPAPF@SiO_2 NPs-PSS(-) ([NPAPF] = 5 μM) at 4 °C for 6 h. HeLa cells were pre-incubated with different inhibitors of chlorpromazine (CPZ, 20 μg/mL) to prevent the formation of clathrin vesicles, cytisine (2 μg/mL) to block caveolae pathway, and amiloride (50 mM) to inhibit macropinocytosis at 37 °C for 1 h. The group incubated with NPAPF NPs without inhibitors treatment was used as the control. After 1 h, the inhibitor solutions were removed, and the NPAPF NPs in media containing inhibitors at the same concentrations were added and further incubated at 37 °C for 6 h. Cells were washed with cold PBS for three times, and fixed with fresh 4% paraformaldehyde for 5 min at room temperature. After that they were visualized

under CLSM. The fluorescence intensities were also measured by flow cytometry for quantitative analysis.

2.9. Intracellular fate of NPAPF NPs

HeLa cells were seeded in glass dishes and cultured for 24 h, and then incubated with NPAPF NPs and NPAPF@SiO_2 NPs. After 6 h, dye NPs were removed. LysoTracker Green (100 nM) was added in medium for additional 30 min at 37 °C following the supplier's protocol. Cells were rapidly washed with fresh medium to remove the attached LysoTracker Green. Finally, living cells were prepared for visualization under CLSM.

The excretion of NPAPF NPs was investigated by CLSM and flow cytometry. In brief, HeLa cells were dispersed in 24-well plates (for CLSM study) and 6-well plates (for flow cytometry analysis) and cultured for 24 h at 37 °C. Then they were incubated with NPAPF NPs and NPAPF@SiO_2 NPs, after 12 h, and transferred to dye-free culture medium and incubated for additional 12 and 24 h. Confocal images were finally taken by CLSM and quantitative data were obtained through flow cytometry.

3. Results and discussion

3.1. Preparation and characterization of NPAPF NPs and NPAPF@SiO_2 NPs

Near infrared reflection (NIR) dye bis(4-(N-(2-naphthyl) phenylamino) phenyl)-fumaronitrile (NPAPF) was chosen in our study. NPAPF NPs were prepared by a simple solvent exchanging method. Then, the as-prepared NPAPF NPs were coated with a thin layer of the silica shell by a modified Stöber method (Scheme in **Fig. S1**)

[15]. The characterization results were summarized in **Table S1**. Specifically, scanning electron microscopic (SEM) image in **Fig. S2a** shows that the NPAPF NPs are spherical and have diameters in the range of 70-100 nm. TEM image in **Fig. 1a** indicates that the NPAPF NPs have a smooth and flat surface. In comparison, after surface modification of these NPs with a thin layer of mesoporous silica nanoshell, the surface has numerous small features over the whole NPs (**Fig. 1b** and **1c**), similar to that of enveloped-spike structure in some viruses [16,17]. DLS studies show that the nude NPs have good dispersibility with an average diameter of about 90 nm and negative ζ potentials of about -22.4 mV, while the average diameter of the modified core-shell structure NPs show a small swelling in diameter (around 110 nm) with a positive ζ potentials of about +17.8 mV (**Fig. S2b** and **2c**). The optical properties of the

nude and modified core-shell structure NPs were then investigated. NPAPF is a kind of dye with the characteristic of AIEE, we studied the optical properties of the as-prepared NPs. As shown in **Fig. 1d**, NPAPF is weakly fluorescent when dissolved in THF, whereas the NPs show almost 10 times enhancement in fluorescence intensity at the same concentration, due to the aggregation-induced restriction of intramolecular rotation and consequential suppression of nonradiative path ways [18]. The modified core-shell structure NPs show similar emission bands with nude NPs, with an intense NIR fluorescence emission peak at 650 nm (**Fig. 1d**). Notably, the fluorescence intensity of the core-shell structure NPs is slightly higher than that of the nude NPs at the same concentration. We assume that the enhanced emission property can be possibly attributed to the reason that a thin layer coating of silica nanoshell over the

nude NPs would make much closer aggregation of the AIEE molecules in the NPs and thus causes the fluorescence enhancement [19]. Similarly, 2-tert-butyl-9,10-di(naphth-2-yl)anthracene (TBADN) NPs were also prepared and modified with a thin layer of SiO_2 coating. The difference is that TBADN has a characteristic of aggregation-induced quenching (AIQ). As shown in **Fig. S3d**, TBADN exhibits strong fluorescence in THF but when they aggregate into NPs the fluorescence quenched dramatically. The nude TBADN NPs are also spherical (**Fig. S3a**) and possess a very smooth surface (**Fig. S3b**). After mesoporous silica nanoshell coating, clearly, the modified NPs hold a large population of small protrusion features on the surface (**Fig. S3c**). DLS measurements show that the sizes of the NPs before and after SiO_2 modification are about 90 and 120 nm, respectively (**Fig. S3e**). However, differently, the fluorescence intensity of the modified TBADN@SiO_2 NPs declines in comparison with that of the unmodified ones when the concentration remains the same (**Fig. S3f**).

3.2. Cellular uptake of various NPs with different surface properties

The different types of NPs were then explored as biological fluorescent probes for cellular imaging. Before that, standard 3-(4,5-dimethylthiazol-2-yl)-2,5-diphenyltetrazolium bromide (MTT) assays were performed in HeLa cell lines to evaluate the cytotoxicities of NPAPF NPs(-), NPAPF NPs-PEI(+), NPAPF@SiO_2 NPs(+) and NPAPF@SiO_2 NPs-PSS(-) (**Fig. S4**). The results show that the cells retain high viabilities (> 85%) after 48 h incubation with the NPs of varied concentrations ranging from 1.25 to 20 μM. It suggests that these NPs have very low cytotoxicity. As shown in **Fig. 2a**, NPAPF@SiO_2 NPs appear to exhibit strikingly brighter fluorescence

than that of NPAPF NPs under the same incubation conditions in human cervical cancer cell lines (HeLa cells). Although the fluorescence intensity of NPAPF@SiO_2 NPs is already confirmed to be higher than that of NPAPF NPs at the same conditions (**Fig. 1d**), this should not be the full reason for the remarkable fluorescence enhancement in *in vitro* imaging. To exclude the influence of the improved fluorescence intensity of the modified NPAPF NPs, we also investigated the cellular uptake of TBADN NPs and TBADN@SiO_2 NPs. As presented in **Fig. 2b**, it is very clear that the TBADN@SiO_2 NPs with core-shell structure still show significantly stronger fluorescence than the TBADN NPs although the modified TBADN NPs actually possess decreased fluorescence intensity. These results imply that the enhanced fluorescence imaging of the NPAPF@SiO_2 NPs is not simply benefited from the enhanced fluorescence after the modification.

Except the change of the surface structure of NPAPF after modification, the other difference is that the modified NPAPF NPs carry positive surface charge while the unmodified ones have negative charge. Therefore, it is also essential to investigate the influence of the surface charge on the cellular uptake of these NPs. To do this, we next examined the cellular delivery performance of NPAPF NPs. To systematically evaluate the influence of surface charge, we further surface modified NPAPF NPs by polyethylenimine (PEI) and NPAPF@SiO_2 NPs by poly(sodium-p-styrenesulfonate) (PSS), named as NPAPF NPs-PEI(+) and NPAPF@SiO_2 NPs-PSS(-), respectively. These two types of NPs have similar values of ζ potential but with opposite charge (**Fig. S2c**). The ζ potentials of raw NPAPF NPs, SiO_2 encapsulated NPAPF NPs, PEI

modified NPAPF NPs and PSS modified NPAPF@SiO_2 NPs are -22.4, +17.8, +20.9, and -19.9 mV, respectively.

In our experiments, the four kinds of NPAPF NPs were individually incubated with HeLa cells for 2, 4, and 6 h. As shown in **Fig. 3a**, rather weak signals are detected in NPs(-) cultured cells, while slightly stronger fluorescence signals are observed for NPs-PEI(+), indicating that positively charged surface of NPs can enhance cellular uptake to some extent. These results are consistent with previous findings that positively charged surface can improve intracellular delivery [20,21]. This is possibly due to the fact that NPs with positive surface charge can be more effectively internalized by cells through electrostatic interactions with the negatively charged cell plasma membrane [22]. In a sharp contrast, strikingly brighter fluorescence signals are seen in HeLa cells cultured with either NPAPF@SiO_2 NPs(+) or NPAPF@SiO_2 NPs-PSS(-). No obvious difference in fluorescence signals can be seen between the two samples with opposite surface charge from confocal microscopy images, especially when cells are incubated for 4 h or longer. Similarly, in human nasopharyngeal epidermal carcinoma cell lines (KB cells), it is also demonstrated that TBADN NPs with surface modification of SiO_2 can more efficiently enter cells than TBADN NPs without surface treatment (**Fig. S5**). These results demonstrate that the positive charge of NPAPF NPs can increase their cell internalization, but the silica nanoshell coating allow the NPs to achieve much higher delivery efficiency no matter what the surface charge is.

The above results are further verified through quantitative measurements of the fluorescence in HeLa and KB cells by flow cytometry (**Fig. 3b, c** and **S6**). The results

show that, after 6 h incubation, the cellular uptake increases almost 10 times for both NPAPF@SiO_2 NPs(+) and NPAPF@SiO_2 NPs-PSS(-) when compared to that of NPAPF NPs(-). In contrast, the cellular uptake improves only 3 times for NPAPF NPs-PEI(+). Clearly, NPAPF@SiO_2 NPs(+) demonstrate the highest cellular uptake. These results verify that the impact of nanoshell silica coating is generic and independent of surface charges and cell lines. Although it is confirmed that positive surface charge is able to increase cellular internalization of NPs, the effect is relatively weak when compared with that of silica nanoshell coating, as observed from **Fig. 3** and **S6**.

It is well known that the effect of nanoparticles adsorption of proteins will also affect their cellular uptake efficiency. When bound to proteins, NPs may be quickly cleared by macrophages before they can reach target cells [23,24]. So, in order to investigate that whether the adsorption of proteins affect cellular internalization of NPs, we test NPAPF NPs with different surface properties on adsorption of BSA (**Fig. S7**). The result indicated that NPAPF NPs having positive zeta potential displayed the highest protein adsorption ability while the negatively charged NPs (especially for NPAPF@SiO_2 NPs-PSS(-)) did not significantly adsorb protein. However, NPAPF@SiO_2 NPs-PSS(-) still possess much higher cellular uptake than that of NPAPF NPs-PEI(+). This result rules out the possibility that the adsorbed proteins induced the higher cellular internalization of NPAPF@SiO_2 NPs. Base on all these observations, we can conclude that the silica nanoshell plays the most important role in boosting the imaging brightness in cells.

3.3. Pathways of the internalization of different NPAPF NPs into cells

To understand why the silica nanoshell coating of NPs can dramatically increase their cellular uptake, it is useful to explore the pathways of their internalization into cells and also compare with NPAPF NPs with different surface properties. For this, we investigated the specific endocytotic pathways that involved in the cellular internalization (**Fig. 4**). First, HeLa and KB cells were pre-incubated at low temperature (4 °C) and then treated with NPs to inspect their energy dependence. Marked decreases in the cellular internalization of all types of NPs (above 85% compared with untreated cells) are observed, indicating that all the internalization is an energy-dependent process. Second, three groups of cells were treated separately with three biochemical inhibitors of clathrin-mediated endocytosis (chlorpromazine, CPZ), caveolae-mediated endocytosis (cytisine), and macropinocytosis (amiloride) to determine the specific cellular uptake mechanism. As shown in **Fig. 4a**, CPZ and cytisine retarded the cellular uptake of NPAPF NPs(-) and NPAPF NPs-PEI(+) to different extents. To acquire more intuitive results, the inhibition efficiencies were then quantitatively measured using flow cytometry. When HeLa and KB cells were pre-incubated with CPZ, cytisine and amiloride, the reduced extents of cellular uptake are 35%, 50%, and 6% respectively for NPAPF NPs(-), and 40%, 20%, and 12% respectively for NPAPF NPs-PEI(+) (**Fig. 4b** and **4c**). In a sharp comparison, no obvious decrease is discerned for NPAPF@SiO_2 NPs(+) and NPAPF@SiO_2 NPs-PSS(-) for both HeLa and KB cells with treatment of three types of inhibitors. From these observations, it could be concluded that the internalization of NPAPF NPs(-) or NPAPF NPs-PEI(+) is mediated by combined pathways of clathrin- and caveolae-mediated endocytosis. The caveolae-mediated

process is the primary endocytosis pathway for NPAPF NPs(-), while the clathrin-mediated process is the main endocytosis pathway for NPAPF NPs-PEI(+) [25,26]. In contrast, clathrin- and caveolae-independent endocytosis most probably plays a crucial role for the uptake of NPAPF@SiO_2 NPs(+) and NPAPF@SiO_2 NPs-PSS(-). It has been previously demonstrated that caveolae- and clathrin-mediated endocytosis are relatively slow in most cells, with half-life ($t_{1/2}$) of more than 20 and 1 min, respectively [27]. Oppositely, recent studies on neuroendocrine cells show that clathrin-independent endocytosis occurs much faster with a half-life of less than 10 s. These results indicate that the silica nanoshell coating allows NPs to enter the tested cells through different pathway from those without a layer of SiO_2. This could make NPAPF@SiO_2 NPs(+) and NPAPF@SiO_2 NPs-PSS(-) transport to cells much easier than NPAPF NPs(-) and NPAPF NPs-PEI(+). Therefore, the unique endocytotic pathways of silica nanoshell coated NPs are responsible for the improved brightness in imaging [28].

3.4. Intracellular fate of NPAPF NPs

Understanding the intracellular localization within the lysosomal network and the fate of NPs are crucial in designing new bioimaging nanomaterials. Such information is also important to confirm the investigated endocytosis pathways of NPs. To study the cellular fate of the NPs following their uptake, the lysosomal compartment of the cultured HeLa cells was stained with the LysoTracker Green probe [29]. The results are shown in **Fig. 5a** and **5b**, the large number of yellow spots in the merged images indicates extensive colocalization of NPs and lysosomes. This finding suggests that the nude NPs mainly be entrapped within lysosomes during incubation. In contrast,

particularly low colocalization ratio is observed for NPAPF@SiO_2 NPs throughout the observation period. The low extent of colocalization with lysosome indicates that NPs with silica coating surface either possess high lysosomal escaping capability or mainly follow other endocytic pathways unrelated to the lysosomal one. In fact, it has been previously reported that nanomaterials utilizing clathrin- and caveolae-independent endocytosis pathway can avoid endo/lysosomal capture and degradation and therefore have significant applications for delivery of anticancer drugs or long-time imaging [30]. After studying the distribution of NPAPF NPs within cells, we investigated their excretion from cells. In the experiments, HeLa cells were first exposed to NPAPF NPs or NPAPF@SiO_2 NPs for 12 h. Subsequently, the cells were washed and incubated with fresh cell medium for additional 6, 12, and 24 h followed by observation by confocal microscopy. The results are presented in Fig. 5c, it is found that the fluorescence intensity of nude NPs sharply reduces. This implies that a large portion of the nude NPs was excreted from the cells. However, the cells with NPAPF@SiO_2 NPs still remain strongly fluorescent without obvious decrease in intensity, showing that most of the NPAPF@SiO_2 NPs stably reside within the cells. These results are further confirmed by quantitative flow-cytometry data (Fig. 5d). The data show that more than 45% of the nude NPs were excreted after the "washed out'' process after 24 h, while only 15% of NPs@SiO_2 were excreted by cells. NPs@SiO_2 stayed in cytosol should be responsible for their low excretion by cells [31]. Similarly, Chu and co-workers recently also revealed that NPs with sharp edges at surface could pierce the membranes of endosomes and escape to the cytoplasm, which in turn

significantly reduced the cellular excretion rate of the NPs [13]. Such features are essential for their application in long-time tracking in bioimaging.

4. Conclusion

In summary, we systematically investigated the influence of silica nanoshell coating on the cell internalization, intracellular transport pathway, intracellular fate, and excretion of NPAPF dye NPs. Surface silica nanoshell coating can dramatically induce over ten-fold enhancement in fluorescence signals in imaging compared with original NPs, indicating their great potential for highly effective cellular imaging. The silica nanoshell coating plays a more predominant role to determine the behaviour of the NPs. NPAPF@SiO_2 NPs enter cells more efficiently and adopt a unique clathrin- and caveolae-independent endocytosis pathway, while NPAPF NPs with other surfaces are internalized into cells through combination of clathrin- and caveolae-mediated endocytosis. As a result, these mesoporous silica nanoshell coated NPAPF NPs mostly bypass the lysosomal compartments and retain in cells for a much longer time. These differences can be summarized in Scheme 1. The combined merits of enhanced cellular uptake efficacy and decreased cellular excretion endow the fluorescent dye NPs with superior imaging performance, which holds great potential for highly sensitive bioimaging, particularly for real-time and long-term tracking of cells.

Acknowledgements

This work was supported by the National Basic Research Program of China (2013CB933500); National Natural Science Foundation of China (Grant No.

61422403, 51672180, 51622306, 21673151); Qing Lan Project; Collaborative Innovation Center of Suzhou Nano Science and Technology (NANO-CIC); and the Priority Academic Program Development of Jiangsu Higher Education Institutions (PAPD).

References

[1] S.M. Borisov, Wolfbeis, Chem. Rev. 108 (2008) 423-461.

[2] Y.L. Yang, F.F. An, Z. Liu, X.J. Zhang, M.J. Zhou, W. Li, X.J. Hao, C.S. Lee, X.H. Zhang, Biomaterials 33 (2012) 7803-7809.

[3] Z. Gu, H.L. Zuo, A.H. Wu, Z.P. Xu, J. Controlled Release 213 (2015) E150-E1.

[4] L. Li, W. Gu, J. Chen, W. Chen, Z.P. Xu, Biomaterials 35 (2014) 3331-3339.

[5] X.L. Hu, J.M. Hu, J. Tian, Z.S. Ge, G.Y. Zhang, K.F. Luo, S.Y. Liu, J. Am. Chem. Soc. 135 (2013) 17617-17629.

[6] M.P. Calatayud, B. Sanz, V. Raffa, C. Riggio, M.R. Ibarra, G.F. Goya, Biomaterials 35 (2014) 6389-6399.

[7] A. Verma, O. Uzun, Y.H. Hu, Y. Hu, H.S. Han, N. Watson, S. Chen, D.J. Irvine, F. Stellacci, Nat. Mater. 7 (2008) 588-595.

[8] M. Massignani, C. LoPresti, A. Blanazs, J. Madsen, S.P. Armes, A.L. Lewis, G. Battaglia, Small 5 (2009) 2424-2432.

[9] A. Asati, S. Santra, C. Kaittanis, J.M. Perez, ACS Nano 4 (2010) 5321-5331.

[10]M.A. Shahbazi, P.V. Almeida, E.M. Makila, M.H. Kaasalainen, J.J. Salonen, J.T. Hirvonen, H.A. Santos, Biomaterials 35 (2014) 7488-7500.

[11]J. Cao, X.X. Xie, A.J. Lu, B. He, Y.W. Chen, Z.W. Gu, X.L. Luo, Biomaterials 35 (2014) 4517-4524.

[12]Y.T. Niu, M.H. Yu, S.B. Hartono, J. Yang, H.Y. Xu, H.W. Zhang, J. Zhang, J. Zou, A. Dexter, W.Y. Gu, C.Z. Yu, Adv. Mater. 25 (2013) 6233-6237.

[13]Z.Q. Chu, S.L. Zhang, B.K. Zhang, C.Y. Zhang, C.Y. Fang, I. Rehor, P. Cigler, H.C. Chang, G. Lin, R.B. Liu, Q. Li, Sci. Rep. 4 (2014) 4495.

[14]R.R. Xu, L.M. Huang, W.J. Wei, X.F. Chen, X.H. Zhang, X.J. Zhang, Biomaterials 93 (2016) 38-47.

[15]X.J. Hao, M.J. Zhou, X.J. Zhang, J.Yu, J.S. Jie, C.T. Yu, Chem. Commun. 50 (2014) 737-739.

[16]K. Grunewald, P. Desai, D.C. Winkler, J.B. Heymann, D.M. Belnap, W. Baumeister, Science 302 (2003) 1396-1398.

[17]P. Zhu, J. Liu, J. Bess, E. Chertova, J.D. Lifson, H. Grise, G.A. Ofek, K.A. Taylor, K.H. Roux, Nature 441 (2006) 847-852.

[18]J. Yu, X.J. Zhang, X.J. Hao, X.H. Zhang, M.J. Zhou, C.S. Lee, X.F. Chen, Biomaterials 35 (2014) 3356-3364.

[19]L. Zhang, N. He, C. Lu, Anal. Chem. 87 (2015) 1351-1357.

[20]R.R. Arvizo, O.R. Miranda, M.A. Thompson, C.M. Pabelick, R. Bhattacharya, J.D. Robertson, V.M. Rotello, Y.S. Prakash, P. Mukherjee, Nano Lett. 10 (2010) 2543-2548.

[21]L. Shang, L.X. Yang, J. Seiter, M. Heinle, G. Brenner-Weiss, D. Gerthsen, G.U. Nienhaus, Adv. Mater. Interfaces 1 (2014) 1300079.

[22]C. He, Y. Hu, L. Yin, C. Tang, C. Yin, Biomaterials 31 (2010) 3657-3666.

[23]S. Patil, A. Sandberg, E. Heckert, W. Self, S. Seal, Biomaterials 28 (2007) 4600-4607.

[24]Q.J. He, J.M. Zhang, J.L. Shi, Z.Y. Zhu, L.X. Zhang, W.B. Bu, L.M. Guo, Y. Chen, Biomaterials 31 (2010) 1085-1092.

[25]Harush-Frenkel, E. Rozentur, S. Benita, Y. Altschuler, Biomacromolecules 9 (2008) 435-443.

[26]G. Sahay, J.O. Kim, A.V. Kabanov, T.K. Bronich, Biomaterials 31 (2010) 923-933.

[27]S.D. Conner, S.L. Schmid, Nature 422 (2003) 37-44.

[28]T. Bamigbade, C. Davidson, R. Langford, J. Stamford, Br. J. Anaesth. 79 (1997) 352-356.

[29]H.Y. Nam, S.M. Kwon, H.J. Chung, S.Y. Lee, S.H. Kwon, H. Jeon, Y. Kim, J.H. Park, J. Kim, S. Her, Y.K. Oh, I.C. Kwon, K. Kim, S.Y. Jeong, J. Controlled Release 135 (2009) 259-267.

[30]S.E. A. Gratton, P.A. Ropp, P.D. Pohlhaus, J.C. Luft, V.J. Madden, M.E. Napier, J.M. Desimone, Proc. Natl. Acad. Sci. USA 105 (2008) 11613-11618.

[31]R.E. Yanes, D. Tarn, A.A. Hwang, D.P. Ferris, S. Sherman, C.R. Thomas, J. Lu, A.D. Pyle, J.I. Zink, F. Tamanoi, Small 9 (2013) 697-704.

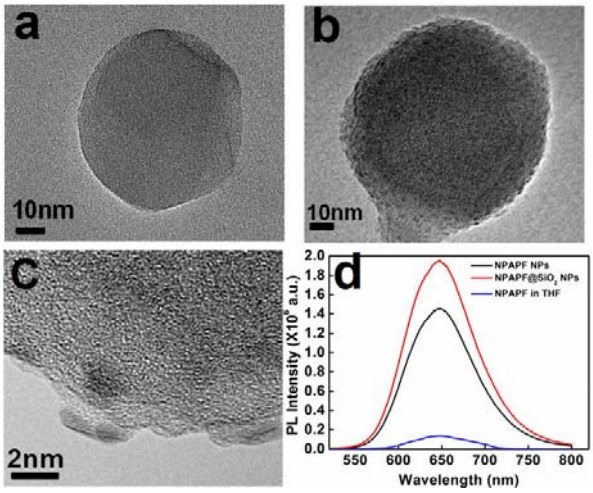

Fig. 1. Characterization of NPAPF NPs. (a) TEM of NPAPF NPs. (b) TEM and (c) HRTEM images of NPAPF@SiO_2 NPs with notably silica shell. (d) Fluorescence spectra of NPAPF NPs and NPAPF@SiO_2 NPs.

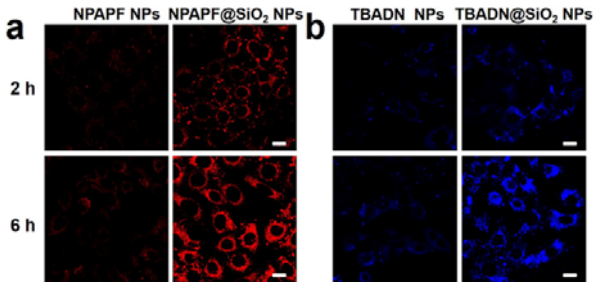

Fig. 2. Confocal microscopy images of HeLa cells incubated with (a) NPAPF NPs, NPAPF@SiO_2 NPs and (b) TBADN NPs, TBADN@SiO_2 NPs for 2 and 6 h at the same concentration. Scale bars: 20 μm.

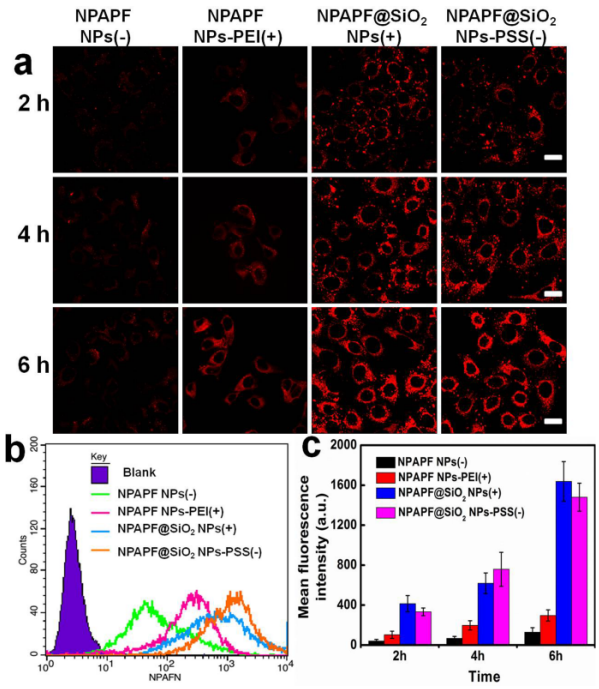

Fig. 3. (a) Confocal microscopy images of HeLa cells incubated with NPAPF NPs(-), NPAPF NPs-PEI(+), NPAPF@SiO_2 NPs(+) and NPAPF@SiO_2 NPs-PSS(-) for 2, 4, and 6 h at the same concentration. The scale bars indicate 20 μm. (b) Flow cytometry analysis of various NPAPF NPs labeled HeLa cells after 6 hours incubation. The colored lines present the distribution of fluorescence intensities. (c) Quantitative measurements of fluorescence intensities in HeLa cells after incubation with NPAPF NPs for 2, 4, and 6 h at the same concentration by flow cytometry.

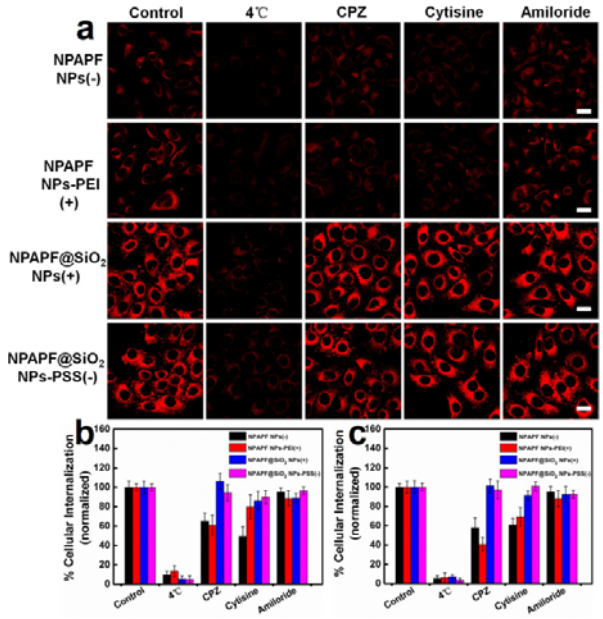

Fig. 4. Effect of added endocytic inhibitors on the internalization of NPAPF NPs. (a) Confocal images showing cellular uptake of NPAPF NPs. Quantitative analysis of the cellular uptake by flow cytometry in (b) HeLa cells and (c) KB cells respectively. Scale bars: 20 μm.

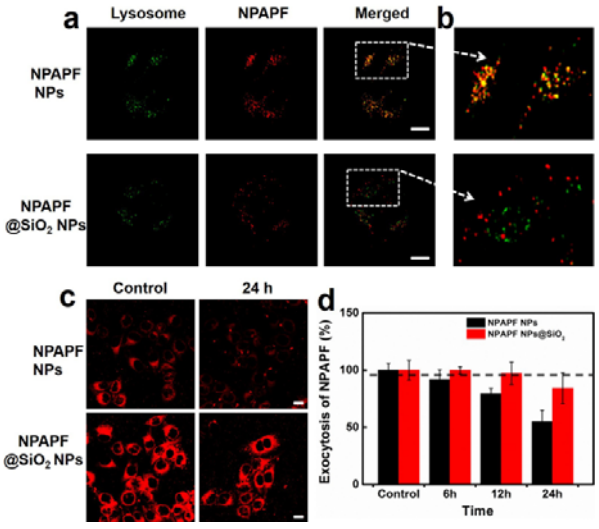

Fig. 5. Colocalization of NPAPF NPs with LysoTracker. (a) Colocalization of NPAPF NPs and NPAPF@SiO_2 NPs with lysosome. (b) Magnified images of the boxed area (white) in (a). (c) Confocal imaging showing the excretion of NPAPF NPs. HeLa cells were incubated for 12 h with NPs and NPAPF@SiO_2 NPs, and then the cells were incubated for additional 24 h in dye-free medium. Scale bar is 20 μm. (d) Quantitative analysis of the cellular excretion by flow cytometry.

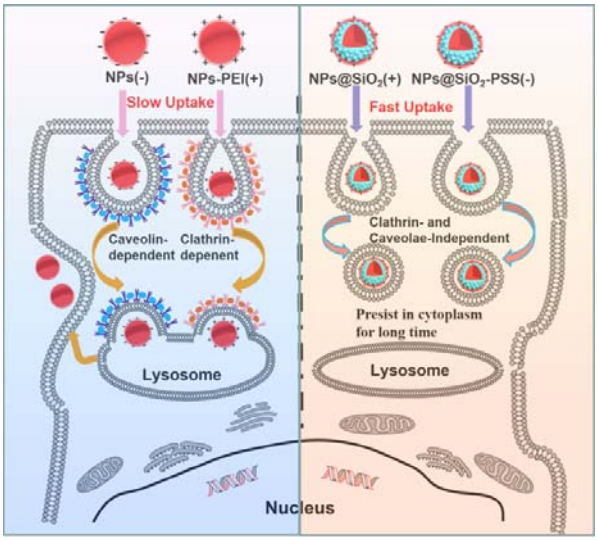

Scheme 1. Schematic illustration of endocytic pathway and the intracellular fate of dye NPs with different surface charge and surface structure.